J Neurophysiol 94: 1636–1644, 2005.
First published April 20, 2005; doi:10.1152/jn.01013.2004.

In Vivo Calcium Imaging of Circuit Activity in Cerebellar Cortex

Megan R. Sullivan,[1,3] Axel Nimmerjahn,[4] Dmitry V. Sarkisov,[2,3] Fritjof Helmchen,[4] and Samuel S.-H. Wang[1,3]
[1]*Departments of Molecular Biology and* [2]*Physics and* [3]*Program in Neuroscience, Princeton University, Princeton, New Jersey; and* [4]*Abteilung Zellphysiologie, Max-Planck-Institut für Medizinische Forschung, Heidelberg, Germany*

Submitted 27 September 2004; accepted in final form 9 April 2005

Sullivan, Megan R., Axel Nimmerjahn, Dmitry V. Sarkisov, Fritjof Helmchen, and Samuel S.-H. Wang. In vivo calcium imaging of circuit activity in cerebellar cortex. *J Neurophysiol* 94: 1636–1644, 2005. First published April 20, 2005; doi:10.1152/jn.01013.2004. In vivo two-photon calcium imaging provides the opportunity to monitor activity in multiple components of neural circuitry at once. Here we report the use of bulk-loading of fluorescent calcium indicators to record from axons, dendrites, and neuronal cell bodies in cerebellar cortex in vivo. In cerebellar folium crus IIa of anesthetized rats, we imaged the labeled molecular layer and identified all major cellular structures: Purkinje cells, interneurons, parallel fibers, and Bergmann glia. Using extracellular stimuli we evoked calcium transients corresponding to parallel fiber beam activity. This beam activity triggered prolonged calcium transients in interneurons, consistent with in vitro evidence for synaptic activation of *N*-methyl-D-aspartate receptors via glutamate spillover. We also observed spontaneous calcium transients in Purkinje cell dendrites that were identified as climbing-fiber-evoked calcium spikes by their size, time course, and sensitivity to AMPA receptor antagonist. Two-photon calcium imaging of bulk-loaded cerebellar cortex is thus well suited to optically monitor synaptic processing in the intact cerebellum.

INTRODUCTION

The molecular layer of the cerebellum is a site of unmatched synaptic divergence. In the rat, the mossy fiber/granule cell pathway consists of nearly 100 million granule cells, each of which extends into the molecular layer a parallel fiber (PF) axon that makes hundreds of synapses onto Purkinje neurons and inhibitory interneurons. These connections re-converge as ~200,000 PF synapses excite each Purkinje cell dendrite (Harvey and Napper 1991). The ~300,000 Purkinje cells send the only axons that project out of the cerebellar cortex. Thus the molecular layer contains the majority of the unitary components of cerebellar processing.

It would be of great interest to monitor the activity of many of these structures simultaneously in living animals. However, most electrophysiological methods allow recordings to be made from only one or a few neurons at a time. In contrast to traditional electrophysiology, two-photon microscopy of fluorescent calcium indicators is well suited for recording from multiple structures simultaneously and has been demonstrated to be an excellent tool for studying neuronal physiology in intact animals (for reviews, see Denk and Svoboda 1997 and Helmchen and Waters 2002).

One limitation of calcium imaging with two-photon microscopy has been the need to use intracellular recording electrodes to fill single neurons with dye, a laborious task. More conveniently, living cells can be loaded in bulk with a membrane-permeant form in which the charged carboxylate groups on indicator dyes are covered by acetoxymethyl (AM) ester groups, which are removed by intracellular hydrolases and esterases (Tsien 1999). This loading approach has been applied to brain slices (Regehr and Tank 1991; Yuste 2000) and more recently to intact animals, in the mammalian brain (Nimmerjahn et al. 2004; Ohki et al. 2005; Stosiek et al. 2003) and the zebrafish spinal cord (Brustein et al. 2003). In these previous in vivo experiments, calcium signals were reported from cell bodies only but not in processes.

Here we extend bulk loading of AM calcium indicator to the cerebellar cortex, including labeling and measurements of axons and dendrites. We characterize evoked responses in PFs, recruitment of stellate interneurons, and spontaneous activity in Purkinje cell dendrites. Our results demonstrate that two-photon microscopy and bulk loading of calcium indicators are well suited to record from all principal components of the cerebellar cortex at once, including axons, dendrites, and postsynaptic neurons. This approach provides a means to study neural processing by the cerebellum in vivo.

METHODS

Animal preparation

Experimental procedures were approved by the Princeton University Institutional Animal Care and Use Committee and performed in accordance with the animal welfare guidelines of the Max Planck Society and the National Institutes of Health. Wistar rats (P21–P28) were deeply anesthetized with urethan (1.5 g/kg body wt ip). A deep level of anesthesia was maintained throughout the experiment as confirmed by the lack of a pinch withdrawal reflex and a lack of whisking, and body temperature was maintained around 37°C. A metal plate was fixed to the skull with dental acrylic cement (Helmchen and Waters 2002; Kleinfeld and Denk 2000; Svoboda et al. 1997). The skull was thinned over the lateral cerebellum (coordinates: 1 mm posterior from the occipital bone, 4 mm lateral) (Shambes 1978). Avoiding the large blood vessels between the folia, a small craniotomy (diameter: 2 mm) was made over folium crus IIa and the dura removed.

Two-photon laser scanning microscopy

In vivo calcium imaging was performed using a custom-built two-photon microscope with custom software (R. Stepnoski and M. Müller, Lucent Technologies, Murray Hill, NJ and MPI, Heidelberg, Germany). The tissue was illuminated with a pulsed Ti:sapphire laser (830–840 nm, 80-MHz repetition rate, 100–150-fs pulse width; Mira 900; Coherent, Santa Clara, CA) pumped with a Verdi 10-W laser (Coherent). Excitation light was focused onto tissue using a 40×, NA

Address for reprint requests and other correspondence: S. Wang, Dept. of Molecular Biology, Lewis Thomas Lab., Princeton University, Washington Road, Princeton, NJ 08544 (E-mail: *sswang@princeton.edu*).

The costs of publication of this article were defrayed in part by the payment of page charges. The article must therefore be hereby marked "*advertisement*" in accordance with 18 U.S.C. Section 1734 solely to indicate this fact.

0.8 water-immersion objective (Carl Zeiss, Thornwood, NY). Emitted light was reflected by a 680-nm long-pass dichroic mirror, filtered (green BG39 Schott glass and infrared-blocking filters) and detected using a photomultiplier tube (R3896, R6357, or H7422P-40; Hamamatsu Photonics, Hamamatsu City, Japan).

Labeling procedure

For in vivo loading of calcium indicator (Stosiek et al. 2003), 50 μg Oregon Green 488 BAPTA-1/AM (Molecular Probes, Eugene, OR) was dissolved into 20% (wt/vol) fresh Pluronic F-127 (Molecular Probes) in DMSO (Sigma) to a concentration of 10 mM. For tissue loading, this stock solution was diluted 20-fold into external saline containing (in mM) 135 NaCl, 5.4 KCl, 1 $MgCl_2$, 1.8 $CaCl_2$, 5 HEPES, and 0.08 Alexa 594. The loading solution was made immediately prior to the injection, spun through a 0.22-μm pore filter to prevent clogging and kept on ice until use. Borosilicate glass micropipettes were pulled (long shank, 5–8 MΩ), filled with 5 μl of the indicator solution and inserted slowly into the cerebellum with a positive pressure of 0.3 bar. Once the micropipette was lowered to 200–250 μm, near the Purkinje cell layer, the pressure was turned up to 1.0 bar for 2 min. After injection, the micropipette was slowly retracted from the tissue. Usually two to three separate injections were made in neighboring locations. After loading, the craniotomy was covered with agarose (1.5%, type III-A, Sigma) dissolved in external saline. A small glass coverslip was positioned over the craniotomy and gently held in place with metal clips to reduce motion due to breathing and heartbeat.

For drug application, a micropipette was filled with 5 μl DL-2-amino-5-phosphonopentanoic acid (APV; 500 μM)/1,2,3,4-tetrahydro-6-nitro-2,3-dioxobenzoquinoxaline-7-sulfonamide (NBQX; 100 μM) or NBQX (100–500 μM) and Alexa 594 (20 μM; Molecular Probes) in external saline. The pipette was inserted into the brain tissue near the optical recording location with no applied pressure. For drug application, 1–1.5 bar of pressure was used for 1–2 min, repeated one to three times. During drug application cell bodies could frequently be seen in negative stain from the Alexa 594.

Data analysis

Ca^{2+} transients were acquired using line scans (64 pixels, 2 ms/line) or full field scans (64 × 64 pixels, 128 ms/frame). Full field movies and line scans were analyzed with MATLAB (MathWorks). Prestimulus background fluorescence from a selected dark region such as a blood vessel was subtracted from each frame.

For analysis of parallel fiber beams, singular value decomposition (SVD), also known as principal component analysis (Jolliffe 1986; Wang et al. 2000b), was used to identify responding pixels. This approach sensitively detects temporally correlated activity shared among different pixels and is resistant to noise-based fluctuations relative to simpler measures such as $\Delta F/F_0$. First, to make the mean value zero for each pixel, a mean intensity image calculated from the entire movie was subtracted from each frame. SVD on the residual signal revealed the calcium response in the first temporal response mode. The additional modes showed no temporal structure and resembled noise. The prestimulus baseline (F_0) and the pattern of response amplitudes were filtered (Gaussian kernel, size = 7 points, $\sigma = 2$). The $\Delta F_{peak,\ SVD}$ contributed by the first mode was calculated by thresholding the response amplitudes and multiplying the result by the peak value of the first temporal mode and first eigenvalue. This quantity is analogous to the traditional ΔF_{peak} but with the noise removed. Data were displayed as $\Delta F_{peak,\ SVD}/F_0$.

Data values are given as means ± SD except as indicated for drug experiments. Spearman correlation coefficients r_s were calculated nonparametrically from rank orders. For purposes of statistical analysis, each imaging location or cell was considered as an independent series, including multiple locations or cells from the same animal. The statistical significance was analyzed using a one-tailed, paired Student's *t*-test except for the drug application experiments which were analyzed with a two-tailed, paired Student's *t*-test.

RESULTS

In vivo calcium indicator loading of cerebellar cortex

We applied a recently introduced method for labeling cell populations with calcium indicators (Stosiek et al. 2003) to the

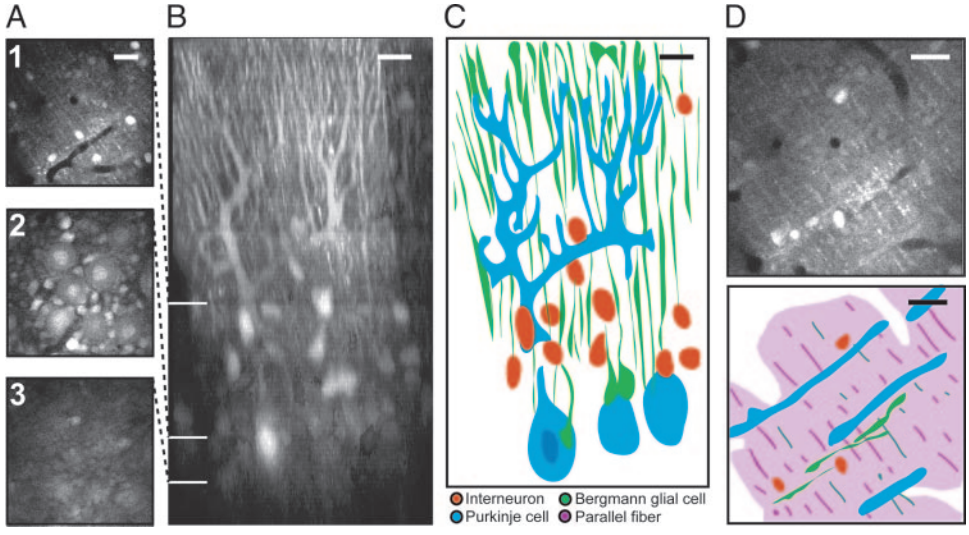

FIG. 1. Calcium indicator labeling in cerebellum. *A*: in vivo 2-photon imaging of cerebellum after labeling with Oregon Green 488 BAPTA-1/AM. Individual raw fluorescence optical sections show the molecular layer (*1*), the Purkinje cell layer (*2*), and the granule cell layer (*3*). Scale bar, 20 μm. *B*: maximum-intensity side projection of 100 optical sections, taken at 2-μm increments, to reconstruct a sagittal view of the labeled cerebellar cortex. The reconstruction begins at the brain surface and extends to the granule cell layer at a depth of 200 μm. The reconstructions allow the identification of the main cell types: interneurons, Purkinje cells, and glia. Scale bar, 20 μm. *C*: diagram of cellular components in *B* showing Purkinje cells in blue, interneurons in red, and Bergmann glia in green. Scale bar, 20 μm. *D*: an enlarged image of the molecular layer demonstrates the variety of labeled structures. The optical section (*top*) was taken at 96 μm below the surface. The diagram (*bottom*) illustrates the main cellular components and the parallel fiber directions are drawn in purple. Blood vessels are unstained and appear as dark structures. Scale bar, 20 μm.

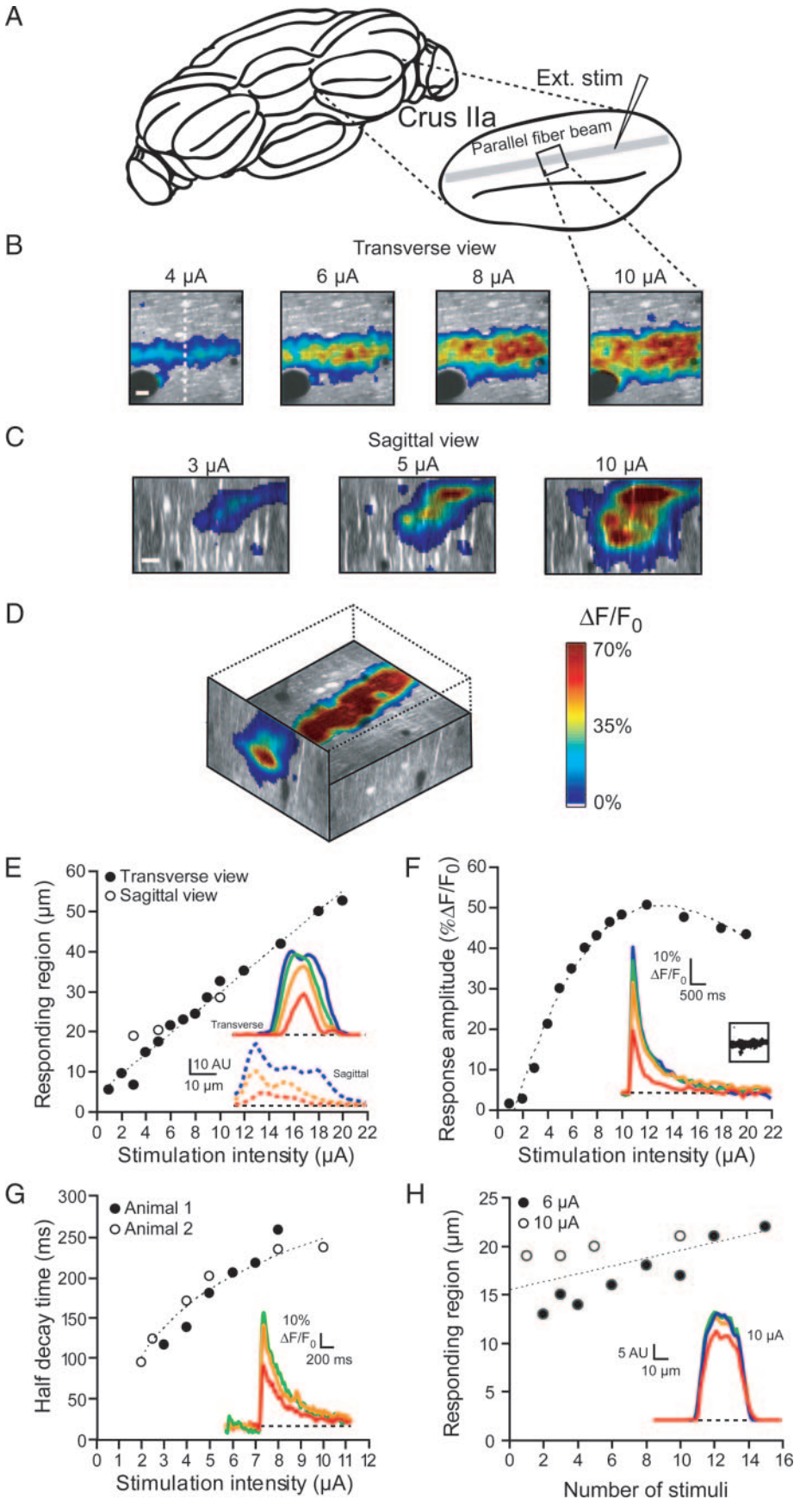

FIG. 2. Evoked calcium transients in parallel fibers. *A*: approximate imaging and stimulus locations. A tungsten stimulating electrode was positioned 100–400 μm away from the imaging site. *B*: a transverse view of the parallel fiber beam showing increases in the width of the response to 5 stimuli delivered at 100 Hz as a function of stimulus intensity. The fluorescence images ($\Delta F/F_0$) were calculated as described in *Experimental procedures*. The vertical dashed line on the far left response indicates the orientation of the sagittal beam views shown in *C*. The stimulating electrode was 55 μm below the surface and 310 μm from the recording site. Scale bar, 10 μm. *C*: a sagittal view of the parallel fiber beam demonstrates an increase in spatial extent as the stimulus intensity increases (25–85 μm below the surface; 310 μm from stimulation electrode; 10 stimuli at 100 Hz; 3–10 μA). The images were reconstructed from a series of line scans over the 60-μm range at increments of 2 μm. Scale bar, 10 μm. *D*: the transverse and sagittal views are combined to show the beam-like fluorescence change observed after extracellular stimulation in the molecular layer (75 μm below the surface; 100 μm from stimulation electrode; 10 stimuli at 100 Hz; 4 μA). The transverse view is shown at the center of the beam. The cross section of the same beam is observed from a sagittal view in the molecular layer (37–107 μm below the surface). The image was reconstructed from a series of sequential line scans taken at depth increments of 2 μm. *E*: the width (*inset, top*: 4–10 μA, 5 stimuli, 100 Hz) and height (*inset, bottom*: 3–10 μA, 10 stimuli, 100 Hz) of the responding region increases linearly with increasing stimulus intensity. The responding region on the *y* axis is defined as the full width at half-maximum. Dashed line is a linear fit. *F*: the maximum amplitude of the beam response increases with stimulus intensity (5 stimuli, 100 Hz). The temporal traces (*inset*) correspond to the beam responses in *B*. The response amplitude was determined using those pixels (*inset*) responding by ≥10%$\Delta F/F_0$ to 4-μA stimulus intensity. Dashed line is a 3rd-order fit. *G*: the half decay time of the parallel fiber calcium transient increased as the stimulus intensity increased (5 stimuli, 100 Hz). The temporal traces (*inset*) correspond to *animal 2* with stimulus intensities of 2, 4, and 5 μA. Dashed line is a logarithmic fit. *H*: the width (*inset*) of the responding region changes little as a function of the number of stimuli (100 Hz). Responses to single stimuli could be observed at higher stimulus intensities (10 μA). The responding region on the *y* axis was defined as in *A*. Dashed line is a linear fit.

intact rat cerebellar cortex. In this paper, we report observations from a total of 39 animals. We pressure-ejected Oregon Green BAPTA-1/AM into folium crus IIa, an easily accessible region in which sensory maps have been made (Bower et al. 1981). Representative optical sections from each of the three layers of the cerebellum showed PFs, interneurons, Purkinje cell bodies, and granule cells (Fig. 1). Purkinje cell dendrites were identified as tube-like structures that ran in directions perpendicular to the PFs and in some cases could be traced down to the Purkinje cell body. The dendrites had a larger diameter (3–6 μm) compared with the other neuronal processes in the imaging field. The deepest clearly resolvable structures we could find were Purkinje cell bodies at a depth of ~200–250 μm. Below this level images appeared blurry and individual granule cells were too dim to resolve well.

In optical sections parallel to the brain surface (Fig. 1*A*; supplemental movie 1)[1] individual PFs were generally not clearly visible. Instead, labeling appeared diffuse, consistent with the fact that PFs are too small and closely spaced to be resolved individually. We did see a subpopulation of exceptionally bright individual structures in the direction of PFs and spaced at regular intervals of ~10 μm that either were heavily labeled PFs or ensheathing glial structures (Castejon et al. 2002). Interneurons were clearly visible as bright spots of 5–10 μm in diameter. Three-dimensional reconstruction produced a sagittal view of loaded tissue (Fig. 1, *B* and *C;* supplemental movie 1) that allowed us to trace Purkinje cell dendrites and Bergmann glial fibers from the Purkinje cell layer and to the pial surface (Palay and Chan-Palay 1974). Separation and tracing of these structures in the reconstructions helped us identify them in the original images (Fig. 1*D*).

Evoked parallel fiber beams

To evoke PF calcium transients, we inserted a tungsten electrode 50–120 μm below the brain surface and delivered current injections. We succeeded in evoking a beam-shaped calcium signal in all 20 animals attempted. Because PFs run longitudinally for nearly 5 mm (Pichitpornchai et al. 1994) we positioned the stimulus electrode ≤400 μm away from the imaging site, a distance limited by the fact that the same craniotomy was used for imaging and to insert the stimulation electrode (Fig. 2*A*).

Focal stimulation with a tungsten electrode (1 MΩ) in the molecular layer using moderate stimuli (1–20 μA, 1–50 stimuli, 100 Hz) evoked fluorescence changes that occurred in narrow bands running along the PF axis (Fig. 2*B*; supplemental movie 2)[1]. The calcium increases evoked in this manner showed a rapid rise (time-to-peak within 1 acquired frame, 0.128 s; 11 imaging locations in 3 animals; 82 trials) and an approximately exponential decay back to baseline [$t_{1/2}$ = 0.34 ± 0.11 (SD) s, 82 trials; $t_{1/2}$ is used throughout the paper as a simple measure of the time course, which was nonexponential in other structures]. These calcium signals resembled presynaptic PF calcium transients measured in vitro (Regehr and Atluri 1995).

From sequential measurements at different focal depths, we could obtain a sagittal view of these responses and reconstruct the three-dimensional extent of PF activation. Figure 2*C* shows a representative example from a total of eight locations imaged in three animals (each location = 18–40 trials). The cross section of the responding beam was mainly disk-shaped but could exhibit irregularities closer to the surface, which might reflect the curvature of the folium near the surface of the brain. Overall we obtained an approximately cylindrical structure (Fig. 2*D*) corresponding to the "beam" described by Eccles (Eccles et al. 1967).

Larger stimulus currents should activate PFs at progressively farther distances from the stimulus electrode. Consistent with this, the width of the beam at half-maximum (full width at half-maximum, FWHM) increased with stimulus intensity from 21 ± 7 μm at 2–4 μA (22 trials) to 38 ± 13 μm at 10 μA (11 trials; 7 locations in 3 animals, 5–10 stimuli, 100 Hz; Fig. 2*E*). Over this range of stimulus currents, increases in width were smooth and monotonic (rank correlation coefficient r_s = 0.99 ± 0.02, $P < 0.0005$ in each of 7 of 7 locations).

Larger stimulus currents might also recruit postsynaptic structures (Eilers et al. 1995; Miyakawa et al. 1992; Wang et al. 2000a). Consistent with this, the maximum amplitude of calcium transients (7 locations in 3 animals) increased with stimulus intensity from 28 ± 5% $\Delta F/F_0$ at 2–4 μA to 57 ± 6% $\Delta F/F_0$ at 10 μA (r_s = 0.97 ± 0.05, $P < 0.0005$ in each of 7 of 7 locations; Fig. 2*F*). Another test of postsynaptic recruitment is the time course of the signal because postsynaptic signals in Purkinje neurons decay more slowly than PF signals (compare Eilers et al. 1995 and Miyakawa et al. 1992 with Regehr and Atluri 1995). For low current intensities (2–3 μA),

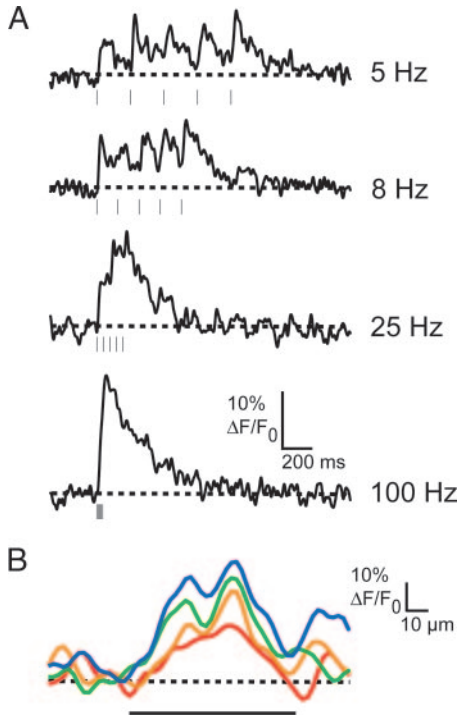

FIG. 3. Temporal limits of detecting evoked calcium signals. *A*: temporal traces showing the evoked parallel fiber responses to different frequencies (5 μA; 5 stimuli at 5–100 Hz). The individual stimulus pulses, designated with the vertical marks below each trace, can be resolved at a frequency ≤25 Hz. *B*: the maximum amplitude of the beam response increases with stimulus frequency. Spatial width profiles from the beam responses shown in *A*. The black line below the profile traces shows the portion of the beam response selected to generate the temporal traces in *A*.

[1] The Supplementary Material for this article (3 movies) is available online at http://jn.physiology.org/cgi/content/full/01013.2004/DC1.

the decay times of the calcium transients ($t_{1/2}$ = 0.27 ± 0.10 s, 5–10 stimuli; 9 trials) were approximately the same as previously reported for brain slices (Regehr and Atluri 1995). With increasing stimulus intensities, the $t_{1/2}$ increased ($t_{1/2}$ = 0.40 ± 0.06 s at 10 μA, 5–10 stimuli, 6 trials; r_s = 0.58 ± 0.20, $P < 0.001$; Fig. 2*G*), consistent with additional postsynaptic recruitment.

Increasing the number of stimuli might increase the beam width by lowering PF stimulus thresholds or by activating spreading postsynaptic signals. However, increasing the number of stimuli (4 locations in 2 animals) led to only a small increase in FWHM beam width (2–3 PF stimuli, 23 ± 5 μm, 4 trials; 10–15 PF stimuli, 27 ± 4 μm, 7 trials; 3–10 μA stimuli, 100 Hz; P = 0.1; Fig. 2*H*). It was also possible to observe beams in response to a single stimulus with moderate stimulus parameters (3–25 μA; 4 locations in 3 animals; 37 trials; data not shown).

To test the temporal limits of signal detection, we varied the stimulus frequency (Fig. 3). Individual transients could be resolved at stimulus frequencies of 3–25 Hz, consistent with in vitro imaging (Regehr and Atluri 1995). At 100 Hz, the individual stimulations summated and it was not possible to resolve the individual calcium transients.

Recruitment of interneurons

Beams of PF activity would be expected to excite stellate and basket interneurons. In 17 animals, we monitored fluorescence in interneuron cell bodies within or near the PF beam. This approach allowed us, for the first time, to monitor activity in multiple interneurons by calcium imaging in vivo. Fluorescence transients in interneurons (225 measurements from 23 different responding cells, 9 locations in 8 animals) had amplitudes comparable to the weaker beam transients (maximum amplitude 27 ± 11% $\Delta F/F_0$) and longer decay times ($t_{1/2}$ = 1.9 ± 1.2 s; $P < 0.001$ compared with beam response) than the beam response (10-μA PF stimulus current; Fig. 4, *A–C*, supplemental movie 3).

Stellate cell dendrites extend for several hundred micrometers sagittally, perpendicular to PF orientation (Palay and Chan-Palay 1974; Sultan and Bower 1998). Consistent with this anatomy, many responding interneurons were found well outside the region of PF beam activation. Responses closer to the beam's center tended to be larger in amplitude and have longer time courses (Fig. 4*B*). Thus PF beam stimulation activates a wide band of interneurons extending well beyond the beam itself.

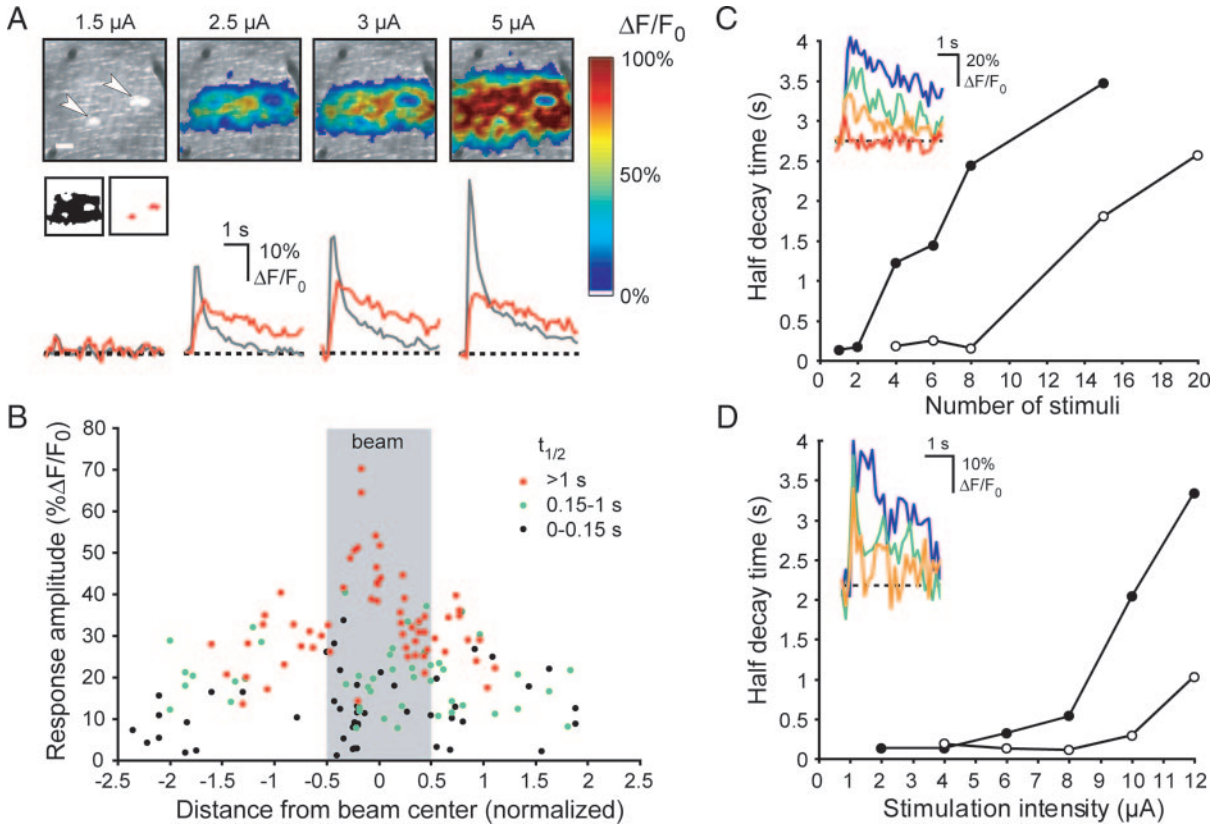

FIG. 4. Recruitment of interneurons. *A*: increases in the size of the parallel fiber beam and recruitment of slower responses in interneurons with increasing stimulus intensity (1.5–5 μA; 10 stimuli at 100 Hz). The 2 interneurons in this frame are indicated with arrows in the response on the *far left*. Recordings were made 120 μm below the surface and 170 μm from the stimulating electrode. Scale bar, 10 μm. Each temporal trace corresponds to the response frame above it, and $\Delta F/F_0$ is calculated directly from pixel intensity averaged from the parallel fiber beam and interneuron regions of interest indicated in the *inset*. The interneuron data, which contain some signal of parallel fiber origin, are shown in red and the parallel fiber beam data are shown in gray. *B*: activation of interneurons both off- and on-beam. Each point shows the maximum response amplitude of an interneuron transient after a PF stimulus train that evoked a measurable beam. The position of each interneuron is plotted relative to the PF beam, indicated in gray. The data represent points from 10 neurons in 2 animals. Interneurons were ≤68 μm from the beam center. Beams were 4–61 μm wide (full width at half-maximum). The colors encode the $t_{1/2}$ of the calcium transients' return to baseline. *C*: the duration of interneuron calcium transients increases with the number of stimuli. Two cells from the same imaging location are shown with filled circles and open circles. The temporal traces (*inset*) correspond to the cell represented by the filled circles. *D*: the duration of interneuron calcium transients increases with stimulus intensity. Two cells are shown from the same imaging location. The temporal traces (*inset*) correspond to the cell represented by the open circles.

Previous in vitro studies have shown that single stimuli to PF beams evoke brief stellate cell responses, whereas trains of stimuli generate prolonged responses lasting for seconds (Carter and Regehr 2000; Clark and Cull-Candy 2002). In 10 responding interneurons ($n = 10$, 3 locations, 2 animals), the PF stimulation parameters were varied systematically (190 trials; PF beams evoked with 2–20 stimuli at 1–20 μA, 100 Hz). At low stimulus intensities (2–4 μA) and brief trains of ≤5 stimuli, interneuron fluorescence transients were small (maximum amplitude = 13 ± 9% $\Delta F/F_0$; 51 trials) and brief (median $t_{1/2}$ 0.13 s, 25–75% quartile range 0.06–0.21 s; mean ± SD: 0.37 ± 0.73 s; 51 trials; Fig. 4, *C* and *D*). With more intense stimulation (8–12 μA, 10–20 stimuli), the transients became larger (maximum amplitude = 27 ± 13%$\Delta F/F_0$, 49 trials; $P < 0.0005$) and the time course of the signals became notably prolonged (median $t_{1/2}$ 0.86 s, 25–75% quartile range: 0.21–2.04 s, mean ± SD: 1.15 ± 1.08 s; 48 trials; $P < 0.0005$; Fig. 4*D*). Within each cell, response amplitude increased with the number of stimuli ($r_s = 0.68 \pm 0.32$, 73 measurements from 9 cells; $P < 0.001$; Fig. 4*C*). Response amplitude also correlated with stimulus intensity ($r_s = 0.77 \pm 0.25$, $P < 0.001$; Fig. 4*D*). The decay time of the interneurons increased with both stimulus number ($r_s = +0.69 \pm 0.30$, 37 measurements from 6 cells, 4 or more responses larger than 20%$\Delta F/F_0$ per cell; $P < 0.001$) and stimulus intensity ($r_s = +0.60 \pm 0.19$, 69 measurements from 10 cells, 4 or more responses larger than 20%$\Delta F/F_0$ per cell, $P < 0.001$).

Prolonged stellate cell responses in vitro are mediated by extrasynaptic glutamate spillover acting on NMDA receptors (Carter and Regehr 2000; Clark and Cull-Candy 2002). If the observed interneuron fluorescence transients in vivo follow the same mechanism, they should be blocked selectively by applying a combination of AMPA- and NMDA-type glutamate antagonists. Local application via a micropipette of a solution containing the NMDA receptor antagonist APV (500 μM) and the AMPA receptor antagonist NBQX (100 μM) to the molecular layer significantly reduced interneuron responses (5 cells from 3 animals) but not PF beam responses (Fig. 5*A*). The maximum amplitude of the interneuron responses decreased from 34 ± 5% $\Delta F/F_0$ (mean ± SE) in control conditions to 23 ± 2% $\Delta F/F_0$ after drug application ($P < 0.05$) while the PF beam was 26 ± 8% $\Delta F/F_0$ in control conditions and 27 ± 6% $\Delta F/F_0$ after drug application ($P = 0.8$).

APV/NBQX also shortened the time course of the interneuron calcium transient (see sample traces in Fig. 5*A*). We quantified the total size of the transient as the area of the interneuron calcium transient, as %$\Delta F/F_0$ summed over multiple frames to give a measurement in units of %$\Delta F/F_0$ frame. The total transient size decreased from 7.5 ± 1.0%$\Delta F/F_0$ frame (means ± SE) to 4.0 ± 0.7%$\Delta F/F_0$ frame with APV/NBQX application ($P < 0.001$). Application of NBQX (100–500 μM; Fig. 5*B*) alone did not significantly attenuate either the amplitude of interneuron responses (25 ± 3%ΔF/F_0 in control conditions, 29 ± 5%$\Delta F/F_0$ after NBQX application, means ± SE, $P = 0.3$, 7 cells from 3 animals) or the total transient size (control total transient size 5.0 ± 0.6%$\Delta F/F_0$ frame, after NBQX application 5.0 ± 0.8%$\Delta F/F_0$ frame, $P = 1.0$; Fig. 5*B*). PF beam responses were not significantly affected by NBQX. Thus consistent with in vitro studies (Carter and Regehr 2000; Clark and Cull-Candy 2002) of extrasynaptic spillover of neurotransmitter, under dense PF stimulation conditions, in vivo responses in interneurons are mediated in part by NMDA receptors, which contribute to the prolonged component of the response.

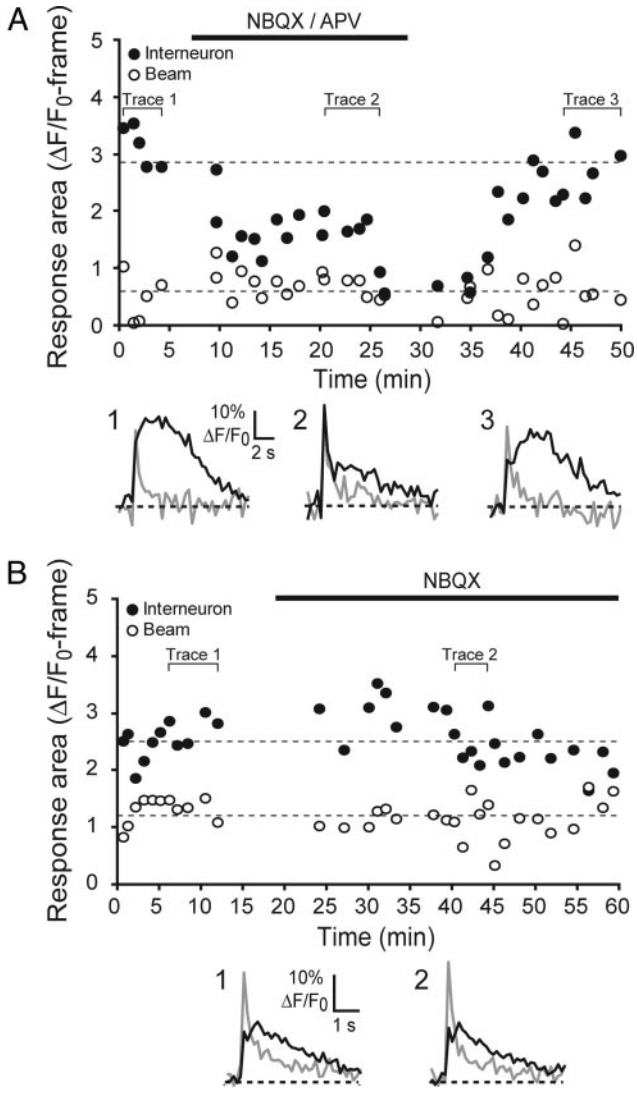

FIG. 5. Pharmacology of parallel fiber-interneuron responses. *A*: the interneuron calcium responses are attenuated with 1,2,3,4-tetrahydro-6-nitro-2,3-dioxobenzoquinoxaline-7-sulfonamide (NBQX) and APV. The effect of NBQX/APV on the parallel fiber beam (open circles) and interneuron (filled circles) is shown over 50 min (10 μA, 10 stimuli, 100 Hz). The temporal traces below the plot are an average of 5 traces obtained prior to NBQX/APV (*1*), while delivering NBQX/APV (*2*), and after removing NBQX/APV (*3*). The interneuron data are in red and the parallel fiber beam data are shown in gray. The horizontal dashed line indicates the mean of either the interneuron (1st 5 and last 5 points) or beam data (all points). *B*: the interneuron calcium responses are not attenuated with NBQX. The effect of NBQX on the parallel fiber beam (open circles) and interneuron (filled circles) is shown over 60 min (1 μA, 5 stimuli, 100 Hz). The temporal traces below the plot are an average of 5 traces obtained prior to NBQX (*1*) and while delivering NBQX (*2*). The horizontal dashed line indicates the mean of either the interneuron (all points) or beam data (all points).

Spontaneous activity in Purkinje cell dendrites

Purkinje cells fire complex dendritic calcium-based action potentials in response to climbing fiber input (Llinás and Sugimori 1980). We therefore looked for signs of spontaneous activity in Purkinje cell dendrites (Fig. 6). We were able to locate

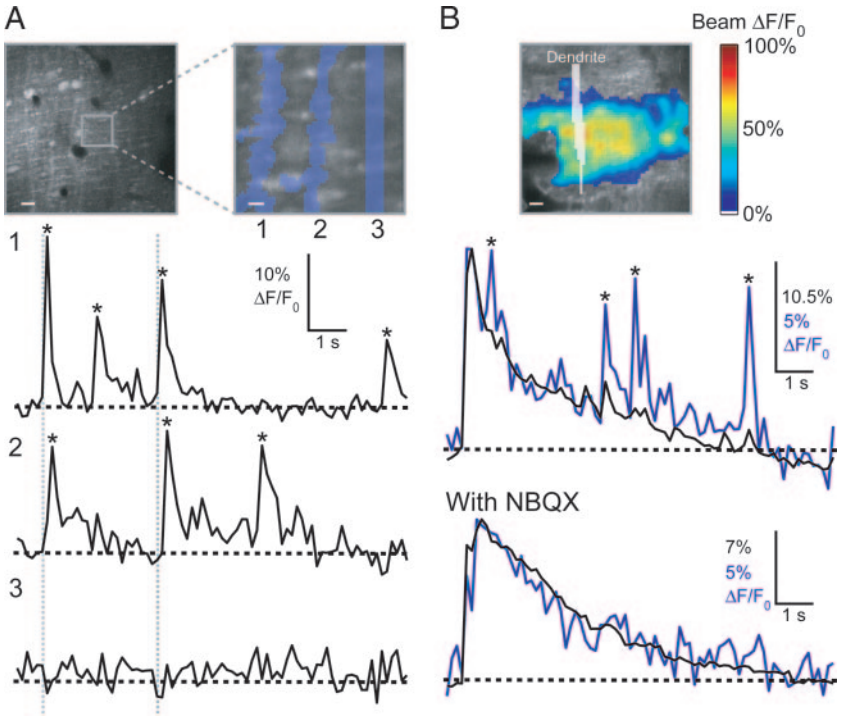

FIG. 6. Purkinje cell dendrites show NBQX-dependent spontaneous activity. *A*: spontaneous activity in neuronal structures can be monitored with high spatial resolution (data taken 75 μm below the brain surface). An overview of the imaged area is shown in the *top left image* (scale bar, 10 um). The right image is a subregion of this area, from which a time series of images was obtained (frame rate, 128 ms; scale bar, 2 um). The spontaneous calcium events are denoted with an asterisk. In correlated events, indicated by gray vertical lines, the response in trace 1 precedes the response in trace 2 by one frame. The blue overlays on the right image show the pixels selected for generating the temporal traces. No signal was observed outside of these areas (trace number 3). *B*: the frequency of spontaneous calcium transients are reduced with NBQX. A raw fluorescence image showing the region has a $\Delta F/F_0$ beam overlay and a white dendrite overlay showing the pixels selected for generating the temporal traces (scale bar, 10 μm). Trace 1 shows a trial 7 min prior to the NBQX application. Trace 2 shows a trial 6 min after the NBQX application. The trials begin with a parallel fiber evoked beam, which remains unchanged with the NBQX application (10 μA, 10 stimuli, 100 Hz). The beam temporal traces are in black and the dendrite temporal traces are in blue.

spontaneous activity in 21 animals. Fast linescans of these spontaneous fluorescence transients showed that the signals rose rapidly and fell with an average half decay time of 0.10 ± 0.07 s (15 dendrites in 3 animals), similar to climbing fiber-evoked signals observed in vitro using high-affinity indicators (Miyakawa et al. 1992). In instances with a field of view of ≥100 μm wide, we could see more than one Purkinje cell dendrite. In neighboring dendrites, spontaneous events sometimes occurred at the same time but not always, suggesting that the transients were evoked by multiple climbing fibers firing in synchrony (Welsh et al. 1995) or that propagation into dendrites was unreliable (Callaway et al. 1995). The rate of spontaneous events was 0.38 ± 0.25 Hz (21 dendrites in 6 animals), similar to reports of spontaneous firing rates for climbing fibers in vivo (Keating and Thach 1997).

Fast synaptic transmission from climbing fiber axons to Purkinje cells occurs via AMPA-type glutamate receptors. In a subset of experiments in which drug was applied, application of the AMPA receptor antagonist NBQX (100–500 μM) decreased the frequency of the spontaneous events in Purkinje cell dendrites from 0.29 ± 0.09 (SE) Hz in control conditions to 0.06 ± 0.03 Hz after NBQX application ($P < 0.05$, 6 dendrites from 3 animals; Fig. 6*B*). A PF-evoked beam signal present at the beginning of each trial as a control could still be evoked after the application of NBQX (see black trace in Fig. 6*B*). In this example, the time course of the remaining beam signal is slower in NBQX and may include postsynaptic AMPA receptor-independent mechanisms such as calcium release (Finch and Augustine 1998; Takechi et al. 1998). Thus blockade of climbing fiber-Purkinje neuron transmission was able to suppress dendritic calcium spiking in vivo.

DISCUSSION

Our observations demonstrate the practicality of simultaneously imaging many signaling components in cerebellar circuitry in vivo by bulk loading of a calcium-sensitive fluorescent dye. In vivo AM loading provides a means of widespread loading that allowed us to resolve neural activity in individual Purkinje cell dendrites and interneurons, and in groups of PFs. These structures constitute the major processing components of the cerebellar cortex. Thus two-photon microscopy is useful for comprehensively monitoring cerebellar activity at multiple stages of processing.

We imaged several types of calcium transients that are likely to reflect physiological mechanisms that previously have been characterized only in cerebellar brain slices. First, parallel fibers (PFs) have been reported to evoke activity in stellate cells via AMPA receptors when single shocks are given, with recruitment of NMDA receptors under burst stimulation (Carter and Regehr 2000; Clark and Cull-Candy 2002). Our observation of prolonged NMDA receptor-dependent calcium signals in response to moderate-intensity PF stimulation indicates that these mechanisms can also be activated in the intact brain. Second, climbing fiber excitation of Purkinje cells leads to dendritic calcium action potentials that do not always succeed in invading the entire dendritic arbor (Callaway et al. 1995). The partial correlation of firing that we saw in adjacent Purkinje cell dendrites is consistent with this type of propagation failure.

While we routinely observed spontaneous Purkinje cell activity, we did not observe spontaneous activity in PFs, a major component of the cerebellar molecular layer. Resolving spontaneous PF signals is, however, a difficult task because signals from individual PFs are likely to be averaged with signals from nearby PFs, considerably reducing the signal-to-noise ratio. A further challenge is presented by the possibility that sensory stimuli may activate only a small number of granule cells (Albus 1971; Chadderton et al. 2004; Marr 1969) and thus a sparse distribution of PFs.

Our PF responses correspond to the concerted activity of several hundred PFs, considerably fewer than the best previous

imaging studies of PF beams (Cohen and Yarom 2000; Gao et al. 2003). In one recent study of in vivo cerebellar plasticity (Gao et al. 2003), extremely strong stimulus parameters (200–300 μA, 10 Hz for 10 s) were used, generating beams that were several hundred micrometers wide. Another study used large stimulating electrodes (diameter = 200 μm) and activated beams of similar size (Cohen and Yarom 2000). Our evoked beams are much more confined in space. In our experiments, the highest stimulus intensity used was 50 μA. At higher intensities we observed oscillations lasting many seconds, suggesting that strong activation of PFs triggers physiologically unrealistic additional events.

Imaging in cerebellum was subject to limits that differed from previous findings in the neocortex. It was not possible to observe any cellular structures below the Purkinje cell layer, ~200–250 μm below the brain surface. Such a shallow limit was surprising because in the cerebral cortex, previous studies imaged to 600 μm below the brain surface (Helmchen and Waters 2002). The inability to resolve granule cells may be due to exceptionally strong light scattering by the small, densely packed granule cells.

In Purkinje cell dendrites, we could resolve action potentials in single neurons. In other structures, signals were resolvable from many structures at once (PFs) or as slower signals in cell bodies (interneurons). However, because bulk labeling with AM-ester dyes is diffuse, it was sometimes difficult to identify individual structures, and we often relied on the structured anatomy of the cerebellum. Additional means of labeling tissue for identification of structures therefore would be highly valuable. This could be achieved by targeting subsets of cerebellar neurons by type or in sparsely distributed populations by expressing either colored fluorescent proteins (XFPs) or fluorescent proteins engineered to act as calcium indicators (Hasan et al. 2004; Miyawaki et al. 2003; Nakai et al. 2001). Similar to a recent report on counterstaining of astrocytes in neocortex (Nimmerjahn et al. 2004), such complementary labeling approaches could be combined with AM-ester dye loading to provide a dual-color label. This would further facilitate the dissection of particular subcellular components. In any case, applied either alone or in combination with other dyes, bulk loading of calcium indicator has the advantage of functionally labeling a wide range of structures, making it the preferred method for monitoring neural processing by ensembles of cerebellar neurons.

ACKNOWLEDGMENTS

We thank B. Kuhn, I. Ozden, S. Shoham, and G. Wittenberg for discussions and for reading the manuscript.

GRANTS

Fellowship support was given by the National Alliance for Autism Research to M. R. Sullivan, from the Böhringer-Ingelheim Foundation to A. Nimmerjahn, and from the Burroughs Wellcome Fund to D. V. Sarkisov. This work was partially supported by the Max Planck Society and by a grant from the National Institutes of Health to S.S.-H. Wang and by a grant from the Human Frontier Science Project to S.S.-H. Wang and F. Helmchen.

REFERENCES

Albus JS. A theory of cerebellar function. *Math Biosci* 10: 25–61, 1971.

Bower JM, Beermann DH, Gibson JM, Shambes GM, and Welker W. Principles of organization of a cerebro-cerebellar circuit. Micromapping the projections from cerebral (SI) to cerebellar (granule cell layer) tactile areas of rats. *Brain Behav Evol* 18: 1–18, 1981.

Brustein E, Marandi N, Kovalchuk Y, Drapeau P, and Konnerth A. "In vivo" monitoring of neuronal network activity in zebrafish by two-photon Ca^{2+} imaging. *Pfluegers* 446: 766–773, 2003.

Callaway JC, Lasser-Ross N, and Ross WN. IPSPs strongly inhibit climbing fiber-activated $[Ca^{2+}]i$ increases in the dendrites of cerebellar Purkinje neurons. *J Neurosci* 15: 2777–2787, 1995.

Carter AG and Regehr WG. Prolonged synaptic currents and glutamate spillover at the parallel fiber to stellate cell synapse. *J Neurosci* 20: 4423–4434, 2000.

Castejon OJ, Dailey ME, Apkarian RP, and Castejon HV. Correlative microscopy of cerebellar Bergmann glial cells. *J Submicrosc Cytol Pathol* 34: 131–142, 2002.

Chadderton P, Margrie TW, and Hausser M. Integration of quanta in cerebellar granule cells during sensory processing. *Nature* 428: 856–860, 2004.

Clark BA and Cull-Candy SG. Activity-dependent recruitment of extrasynaptic NMDA receptor activation at an AMPA receptor-only synapse. *J Neurosci* 22: 4428–4436, 2002.

Cohen D and Yarom Y. Cerebellar on-beam and lateral inhibition: two functionally distinct circuits. *J Neurophysiol* 83: 1932–1940, 2000.

Denk W and Svoboda K. Photon upmanship: why multiphoton imaging is more than a gimmick. *Neuron* 18: 351–357, 1997.

Eccles JC, Ito M, and Szentágothai J. *The Cerebellum as a Neuronal Machine.* Berlin: Springer-Verlag, 1967.

Eilers J, Augustine GJ, and Konnerth A. Subthreshold synaptic Ca^{2+} signalling in fine dendrites and spines of cerebellar Purkinje neurons. *Nature* 373: 155–158, 1995.

Finch EA and Augustine GJ. Local calcium signalling by inositol-1,4,5-trisphosphate in Purkinje cell dendrites. *Nature* 396: 753–756, 1998.

Gao W, Dunbar RL, Chen G, Reinert KC, Oberdick J, and Ebner TJ. Optical imaging of long-term depression in the mouse cerebellar cortex in vivo. *J Neurosci* 23: 1859–1866, 2003.

Harvey RJ and Napper RMA. Quantitative studies on the mammalian cerebellum. *Prog Neurobiol* 36: 437–463, 1991.

Hasan MT, Friedrich RW, Euler T, Larkum ME, Giese G, Both M, Duebel J, Waters J, Bujard H, Griesbeck O, Tsien RY, Nagai T, Miyawaki A, and Denk W. Functional fluorescent Ca^{2+} indicator proteins in transgenic mice under TET control. *PLoS Biol* 2: e163, 2004.

Helmchen F and Waters J. Ca^{2+} imaging in the mammalian brain in vivo. *Eur J Pharmacol* 447: 119–129, 2002.

Jolliffe IT. *Principal Component Analysis.* New York: Springer-Verlag, 1986.

Keating JG and Thach WT. No clock signal in the discharge of neurons in the deep cerebellar nuclei. *J Neurophysiol* 77: 2232–2234, 1997.

Kleinfeld D and Denk W. *Two-Photon Imaging of Neocortical Microcirculation.* Cold Spring Harbor, NY: Cold Spring Harbor Laboratory Press, 2000.

Llinás R and Sugimori M. Electrophysiological properties of in vitro Purkinje cell dendrites in mammalian cerebellar slices. *J Physiol* 305: 197–213, 1980.

Marr D. A theory of cerebellar cortex. *J Physiol* 202: 437–470, 1969.

Miyakawa H, Lev-Ram V, Lasser-Ross N, and Ross WN. Calcium transients evoked by climbing fiber and parallel fiber synaptic inputs in guinea pig cerebellar Purkinje neurons. *J Neurophysiol* 68: 1178–1189, 1992.

Miyawaki A, Mizuno H, Nagai T, and Sawano A. Development of genetically encoded fluorescent indicators for calcium. *Methods Enzymol* 360: 202–225, 2003.

Nakai J, Ohkura M, and Imoto K. A high signal-to-noise Ca^{2+} probe composed of a single green fluorescent protein. *Nat Biotechnol* 19: 137–141, 2001.

Nimmerjahn A, Kirchhoff F, Kerr JND, and Helmchen F. Sulforhodamine 101 as a specific marker of astroglia in the neocortex in vivo. *Nat Methods* 1: 31–37, 2004.

Ohki K, Chung S, Ch'ng YH, Kara P, and Reid RC. Functional imaging with cellular resolution reveals precise micro-architecture in visual cortex. *Nature* 433: 597–603, 2005.

Palay SL and Chan-Palay V. *Cerebellar Cortex: Cytology and Organization.* Berlin: Springer, 1974.

Pichitpornchai C, Rawson JA, and Rees S. Morphology of parallel fibres in the cerebellar cortex of the rat: an experimental light and electron microscopic study with biocytin. *J Comp Neurol* 342: 206–220, 1994.

Regehr W and Atluri PP. Calcium transients in cerebellar granule cell presynaptic terminals. *Biophys J* 68: 2156–2170, 1995.

Regehr WG and Tank DW. Selective fura-2 loading of presynaptic terminals and nerve cell processes by local perfusion in mammalian brain slice. *J Neurosci Methods* 37: 111–119, 1991.

Shambes GM, Gibson JM, and Welker W. Fractured somatotopy in granule cell tactile areas of rat cerebellar hemishperes revealed by micromapping. *Brain Behav Evol* 15: 94–140, 1978.

Stosiek C, Garaschuk O, Holthoff K, and Konnerth A. In vivo two-photon calcium imaging of neuronal networks. *Proc Natl Acad Sci USA* 100: 7319–7324, 2003.

Sultan F and Bower JM. Quantitative Golgi study of the rat cerebellar molecular layer interneurons using principal component analysis. *J Comp Neurol* 393: 353–373, 1998.

Svoboda K, Denk W, Kleinfeld D, and Tank DW. In vivo dendritic calcium dynamics in neocortical pyramidal neurons. *Nature* 385: 161–165, 1997.

Takechi H, Eilers J, and Konnerth A. A new class of synaptic response involving calcium release in dendritic spines. *Nature* 396: 757–760, 1998.

Tsien RY. Monitoring cell calcium. In: *Calcium as a Cellular Regulator*, edited by Carafoli E and Klee CB: Oxford, 1999, 28–54.

Wang SS-H, Denk W, and Häusser M. Coincidence detection in single dendritic spines mediated by calcium release. *Nat Neurosci* 3: 1266–1273, 2000a.

Wang SS-H, Khiroug L, and Augustine GJ. Quantification of spread of cerebellar long-term depression using chemical two-photon uncaging of glutamate. *Proc Natl Acad Sci USA* 97: 8635–8640, 2000b.

Welsh JP, Lang EJ, Suglhara I, and Llinas R. Dynamic organization of motor control within the olivocerebellar system. *Nature* 374: 453–457, 1995.

Yuste R. Loading brain slices with AM esters of calcium indicators. In: *Imaging Neurons: A Laboratory Manual*, edited by Yuste R, Lanni F, and Konnerth A. Cold Spring Harbor: Cold Spring Harbor Laboratory Press, 2000, p. 34.1–34.9.